Bouncing ion clusters in the plasma sheet boundary layer observed by Cluster-CIS

A. Keiling, G. K. Parks, H. Rème, J. Dandouras, J. M. Bosqued, M. Wilber, M. Mccarthy, C. Mouikis, E. Amata, B. Klecker, et al.

Bouncing ion clusters in the plasma sheet boundary layer observed by Cluster-CIS

A. Keiling,[1,2] G. K. Parks,[1] H. Rème,[2] I. Dandouras,[2] J. M. Bosqued,[2] M. Wilber,[1] M. McCarthy,[3] C. Mouikis,[4] E. Amata,[5] B. Klecker,[6] A. Korth,[7] R. Lundin,[8] and H. U. Frey[1]

Received 25 March 2004; revised 1 May 2005; accepted 1 June 2005; published 3 September 2005.

[1] We report on ion beams injected into the plasma sheet boundary layer (at or near the separatrix) at distances >39 R_E and up to 169 R_E that bounced several times back and forth (up to three echoes) while remaining in coherent bunches before thermalizing in the central plasma sheet. These bouncing ion clusters (BIC) interacted with the far-tail current sheet with a possible curvature parameter, κ, of less than 2. The existence of these BIC shows that ion beams can interact several times nonadiabatically with the far-tail current sheet and still remain coherent. Owing to the large-scale $\mathbf{E} \times \mathbf{B}$ drift, echoes also appeared in the central plasma sheet (CPS) after several bounces. The echoes had higher energies compared with the initially injected ion cluster which can be attributed to additional nonadiabatic acceleration during their second and third interaction with the tail current sheet. After multiple bounces, the ion cluster became thermalized isotropic plasma mixing with the CPS. The three BIC events presented here were identified on the basis of the energy dispersion slopes associated with the ions. Simple model calculations showed, however, that in the case of these far-tail ion injections the 1:3:5:etc.-ratios of travel distances for echoes, used as diagnostics for near-Earth adiabatic BIC, are not valid. This is largely due to a significant shortening of the tail field lines, caused by earthward convection, during the large ion travel times. The model calculations also reproduced newly observed properties such as concave dispersion slopes for the echoes. Furthermore, we argue here that the energy dispersion of the BIC was dominated by a time-of-flight effect. The injection region for the three BIC events, determined on the basis of this time-of-flight interpretation, covered broad ranges of ΔX (GSE) = 26–40 R_E. Two BIC events occurred during the substorm recovery phase; the other BIC event occurred during quiet geomagnetic activity. For two BIC events, UV images were available showing that they were magnetically connected to the poleward arc of the double oval. One BIC event was also conjugate to a small active region inside the poleward arc. We conclude that these nonadiabatic BIC are different from the adiabatic BIC that are routinely reported in the CPS.

Citation: Keiling, A., et al. (2005), Bouncing ion clusters in the plasma sheet boundary layer observed by Cluster-CIS, *J. Geophys. Res.*, *110*, A09207, doi:10.1029/2004JA010497.

1. Introduction

[2] Bouncing ion clusters (BIC) are ion formations that travel along Earth's magnetic field lines and bounce back and forth between the northern and southern hemispheres on closed field lines or bounce between one hemisphere and the tail current sheet. BIC show energy dispersion and it is this dispersion which allows their identification. However, if monoenergetic particles are injected, bounces without dispersion could occur in principle, but their identification would be impossible. At least three criteria must be met to detect BIC. First, a mechanism of ion acceleration is required. Second, the accelerated ions must be able to remain long enough in their formation, while traveling on closed field lines, so that their signature remains coherent. Third, to record the bounces (called echoes hereafter) of the initial ion formation, the satellite (or satellites) must be suitably located.

[3] The first observations of BIC in both the dayside and the nightside were made with ATS 5 and 6 which had

[1]Space Sciences Laboratory, University of California, Berkeley, California, USA.
[2]Centre d'Etude Spatiale des Rayonnements, Toulouse, France.
[3]Department of Geophysics, University of Washington, Seattle, Washington, USA.
[4]University of New Hampshire, Durham, New Hampshire, USA.
[5]Instituto di Fisca dello Spazio Interplanetario, Roma, Italy.
[6]Max-Planck-Institut für Extraterrestrische Physik, Garching, Germany.
[7]Max-Planck-Institut für Aeronomie, Katlenburg-Lindau, Germany.
[8]Swedish Institute of Space Physics, Kiruna, Sweden.

0148-0227/05/2004JA010497

geosynchronous orbits [*Quinn and McIlwain*, 1979]. It is now known that BIC are a common signature at geosynchronous orbit. There appears to be consensus that this type of BIC is generated by the convection surge mechanism which impulsively accelerates ions along magnetic field lines during the course of a dipolarizing magnetotail [*Quinn and Southwood*, 1982]. The associated energy dispersion of the BIC is thus due to the time-of-flight effect. Observations and simulations support this mechanism [*Mauk*, 1986].

[4] BIC were also observed away from geosynchronous orbit in other regions of the magnetosphere. Most of these BIC were classified as essentially being of the same type as those occurring at geosynchronous orbit, by showing that dipolarization was occurring simultaneously with the BIC. For example, *Hirahara et al.* [1996] made BIC observations at about 10,000 km altitude using Akebono. The ion source distance was estimated to be 20–30 R_E on the basis of the time-of-flight (TOF) effect. Although most BIC occurred at times of dipolarization, it was pointed out that a few BIC events showed no dipolarization but it was suggested that this was because no satellite was favorably located to observe the dipolarization. It was suggested that these BIC are the low-altitude signature of the BIC first observed by *Quinn and McIlwain* [1979].

[5] BIC have also been recorded in the magnetotail at 10 R_E using Geotail data [*Kazama and Mukai*, 2003]. The observations were also put in the context of the TOF effect on the basis of which the injection location was estimated to be 29 R_E. The main reason for assuming a temporal structure was its temporal coincidence with a dipolarization at Geotail's location, and thus it was also suggested that the convection surge model was causing the acceleration of ions even though the injections occurred far away from the geosynchronous position.

[6] A fundamentally different type of BIC was reported by *Bosqued et al.* [1993], who investigated 101 precipitating dispersed ion structures in the auroral zone at altitudes less than 2000 km (using AUREOL3). It was suggested that these ion structures were on field lines that map to the tail plasma sheet boundary layer (PSBL) and originated in the far tail. For 10 events, secondary ion clusters (i.e., BIC) were detected. All BIC events occurred during substorm recovery phases, i.e., during time periods of no dipolarization, implying a different ion acceleration mechanism from the one mentioned above. Good agreement with the results of a particle simulation [*Ashour-Abdalla et al.*, 1993] led the authors to conclude that neutral sheet acceleration, in the form of Speiser orbits [*Speiser*, 1967], was operating. The authors argued that the dispersed ion structures were quasi-static structures based on the observation that the associated energy dispersion showed a systematic decrease in energy with decreasing latitude.

[7] In a recent Cluster study, one BIC event was reported in the PSBL [*Keiling et al.*, 2004a]. Data from three Cluster spacecraft were used to investigate properties of the initial ion injections. Here we show the same event but improve their analysis of the bouncing signature by comparing the observations with model calculations. This has led to new observational features. We also show additional BIC events, all of which were identified on the basis of the characteristics of the energy dispersion and model comparisons. We will discuss the significance of these observations in the context of adiabatic and nonadiabatic motion in the current sheet. We will conclude that these BIC are different from those that occur on more dipolar field lines and that are associated with the convection surge mechanism.

2. Instrumentation

[8] The observations presented here are from the Cluster spacecraft which are placed in a 57-hour orbit with perigee and apogee of 4 and 19.6 R_E geocentric distance, respectively. Data used in this study come from the Cluster Ion Spectrometry (CIS) instrument [*Rème et al.*, 2001]. CIS consists of two complementary sensors to measure the full, three-dimensional ion distributions with a time resolution of down to 4 s (one spin period). The Composition and Distribution Function (CODIF) analyzer measures the distribution of H+, He+, He++, and O+ in the energy range from ~0 to 40 keV with an angular resolution of 22.5°. The Hot Ion Analyzer (HIA) does not offer mass resolution but has a better angular resolution of 5.6° and an energy range up to 34 keV.

[9] In addition to the Cluster-CIS data, we utilized ground magnetic field data from the International Monitor for Auroral Geomagnetic Effects (IMAGE), the preliminary AE index from the World Data Center for Geomagnetism at Kyoto, and auroral images from the Wideband Imaging Camera of the far-ultraviolet imaging instrument on board the IMAGE spacecraft [*Mende et al.*, 2000].

3. Data Analysis and Model

[10] In this study we use the "1/v-method" together with a comparison of model results to facilitate the identification of BIC. Several studies [e.g., *Hirahara et al.*, 1996; *Kazama and Mukai*, 2003] have used the "1/v-method" to determine some key quantities of energy-dispersed ion structures such as injection time, injection field line, injection distance, or to show their bouncing properties. In principle, the dispersion signature of BIC can be caused by (1) the equatorward $\mathbf{E} \times \mathbf{B}$ drift of quasi-statically injected ions which latitudinally separates ions with different speeds, or (2) the different travel times it takes quasi-simultaneously injected ions with different speeds to reach the spacecraft. The former ion structures are referred to as VDIS (velocity-dispersed ion structures) and the latter as TDIS (time-dispersed ion structures). We refer the reader to *Keiling et al.* [2004a] for a longer description of VDIS and TDIS. For VDIS, the inverse velocity (1/v) versus invariant latitude spectrogram allows the determination of the injection field line by fitting a straight line through the structure and determining the intercept with the 1/v = 0 line. When 1/v is plotted versus time (instead of invariant latitude), the inverse of the slope is (v_D/v_{SC})*d where v_{SC} is the spacecraft speed, v_D is the convection speed of field lines at the spacecraft location (assuming constant speed), and d is the travel distance of the ions. Unless v_D is known, the travel distance cannot be determined directly. For TDIS, the intercept of the slope with 1/v = 0 gives the injection time and the inverse of the slope is the travel distance in inverse velocity versus time spectrograms. Note that in the case of VDIS, if $v_D = v_{sc}$, the same relationship is obtained as for TDIS.

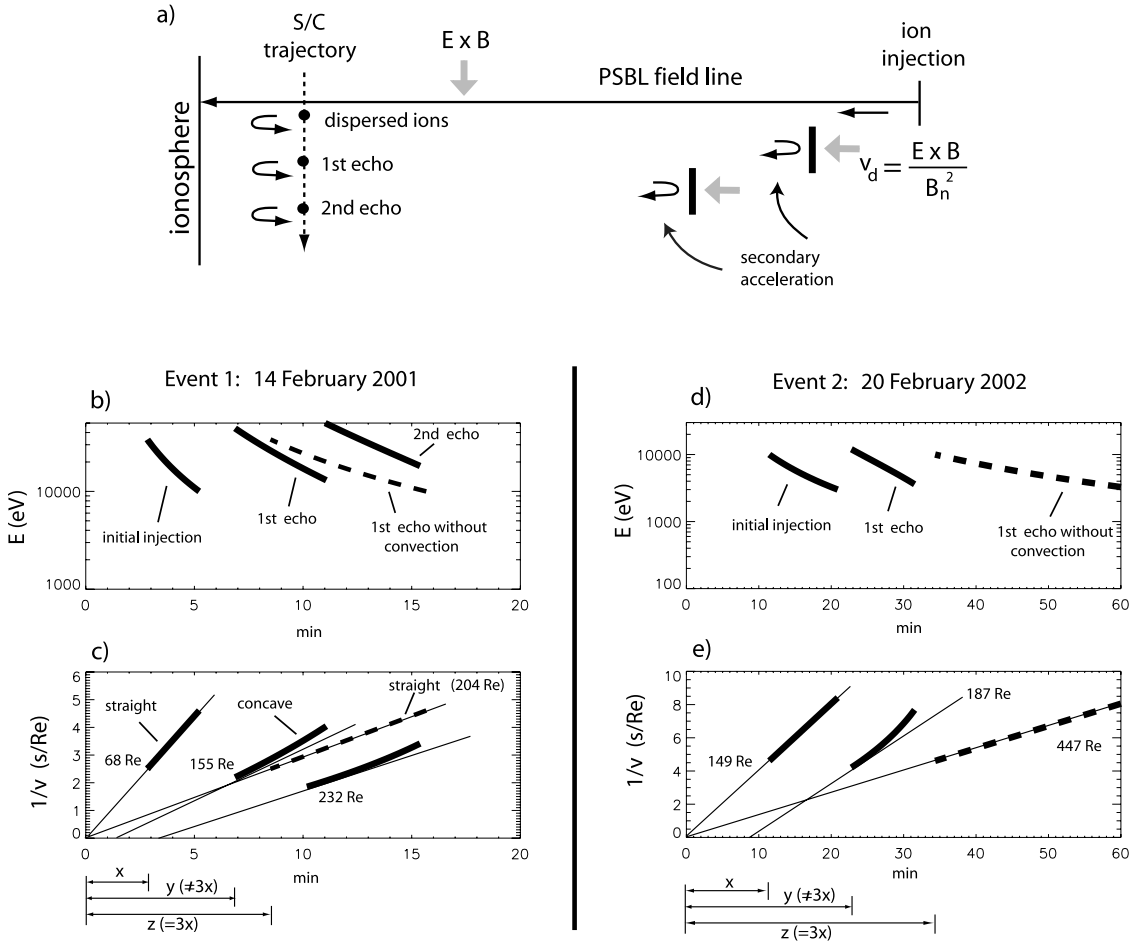

Figure 1. (a) Illustration of the kinematic model to calculate ion dispersion traces of bouncing ion clusters in the plasma sheet boundary layer (PSBL). After acceleration and injection, ions with a broad range of energies travel on field lines toward Earth while also convecting toward the midplane. After passing the spacecraft, the ions mirror below the spacecraft and travel back toward the magnetotail. At the current sheet, the ions turn around and undergo a secondary acceleration. The turning points are closer than the injection location because the field lines convected earthward during the ion travel time. (b) and (c) Model results for an ion injection at 68 R_E (see text for more description). (d) and (e) Model results for an ion injection at 149 R_E.

[11] To identify BIC, the travel distance ratios of 1:3:5:etc. for an initial injection and its echoes have commonly been applied for injections less than 30 R_E away from Earth. However, using a kinematic model, we will show below that these ratios are not appropriate for far-tail injections. This is because of the combination of at least three effects: (1) the earthward convection of tail magnetic field lines (in addition to their equatorward convection) during the ion travel time, (2) the range of energies in the ion cluster, and (3) an additional acceleration of echoes on subsequent returns to the current sheet. The resulting effect is illustrated in Figure 1 for the case of an impulsive acceleration and injection of ions (TDIS) with a broad range of energies onto PSBL field lines. Figure 1a is an illustration of the model, and Figures 1b–1e show results for two different sets of initial parameters.

[12] We now describe the model used to analyze the observed BIC signatures. Owing to the different speeds of ions injected simultaneously in the magnetotail, the spacecraft records an energy dispersion signature at its first encounter with the initial ion cluster. After mirroring at lower altitude, the ions travel back to the magnetotail. In the meantime, the part of the field line that crosses the equatorial plane (i.e., the field reversal region) has convected earthward with speed $v_{d,}$ resulting in a field line shortening. Hence the ions do not reach as far back in the tail as the injection site but instead will turn around in the current sheet at a smaller distance. This distance varies for ions with different energies: slower ions turn around at a shorter distance away from the Earth because the field lines have had more time to convect earthward. Thus it is necessary to consider a changing turning point in the tail which is depicted as a vertical line that moves at speed v_d toward the Earth (Figure 1a). As ions return to the current sheet, they undergo additional acceleration (called secondary acceleration hereafter) in the current sheet [*Ashour-Abdalla et al.*, 1992]. Here we do not model the nonadiabatic dynamics of this secondary acceleration but instead account for it by raising the energy of each ion that returned to the current sheet. Following Speiser-type orbits, the ions again

travel toward Earth. The spacecraft will then record the first echo of the initial ion injection. As time goes on, the spacecraft records on its orbit several echoes of the initial ion injection. How many echoes are observed depends on the orbital speed, the injection properties, and the physical conditions in the magnetotail. Note that the model implements the scenario in which the ions bounce between the ionosphere and the current sheet. An alternative scenario is that the tailward traveling ions cross the current sheet and travel toward the opposite ionosphere. Assuming a bidirectional injection into both hemispheres, both scenarios yield the same ion dispersion signatures at the spacecraft location. The latter scenario is believed to occur for BIC observed on dipolar field lines [*Mauk*, 1986].

[13] Figures 1b and 1c show the model results for a spacecraft (such as Cluster) that encounters BIC in the PSBL. The model parameters were chosen so as to match the observations of the event discussed in section 5.1. Ions with a range of energies (10–34 keV) were injected simultaneously at a distance of 68 R_E. The three solid dispersion lines are, from left to right, the initial ion cluster, the first echo, and the second echo. The dashed line shows, as a comparison, the energy dispersion of an echo that would result if no tail convection and no secondary acceleration occurred in the magnetotail. Transforming the energy-time spectrogram (Figure 1b) into 1/v versus time (Figure 1c) facilitates the analysis, which will also be done for the actual events later. The first ion cluster encounter yields a straight line (Figure 1c). Using the slope to calculate the travel distance gives 68 R_E as expected. Without earthward convection (dashed line), the travel distance of the first echo is 204 R_E, which is three times the injection distance, and the extension of the dashed line (first echo without convection) intercepts the extension of the slope of the initial injection on the line 1/v = 0. This simply indicates that both dispersion traces were caused by the same ions.

[14] In the more realistic case that convection is present in the magnetotail, the echoes show energy dispersion traces that concave upward in the 1/v versus time plots (Figure 1c). The "concaveness" is mostly caused by the combination of earthward convection and the range of ion energies, whereas the displacement of the dispersion traces toward higher energies (smaller 1/v) is caused by the secondary acceleration. For the time period from the first structure to the first echo, we chose a tail convection of v_d = 350 km/s; after that we chose v_d = 180 km/s. The secondary acceleration increased the ion energy by 30–40% for the two echoes. These model input parameters reproduced the observations of the event (14 February 2001) presented in section 5.1. We emphasize that in general convective tail flows are very variable [*Paterson et al.*, 1998], and since there is currently no way to monitor the global flow in detail, we used average values for the convection speeds. A justification for the larger v_d at larger distances (note that the first echo crossed the current sheet at larger distances compared to the second echo) might be that for a monotonically decreasing magnetic field in the magnetotail, the convection speed decreases with decreasing distance from Earth.

[15] The concave dispersion slopes of echoes (Figure 1c) express the fact that ions with different energies traveled different distances since at each time point in the 1/v-plot the corresponding tangent has a different slope. (The reader is reminded that the inverse of the slope value equals the travel distance). Consequently, not one but many different distances are associated with each echo. Here we drew the tangent associated with the most energetic ions. The tangent of the first echo yields a travel distance of 155 R_E which is significantly smaller than 204 R_E which is the travel distance of ions in a magnetotail without convection. Note also that the intercept of the tangent does not coincide with the one of the initial ion structure but instead intercepts the 1/v = 0 line at a later time.

[16] When discussing the nonadiabatic conditions of bouncing ions in the tail current sheet in section 6.3, we need an estimate of where the injected ions return to the current sheet. From the model and the given input parameters (previous paragraph) we find that for example, the 34-keV (10-keV) ions injected at 68 R_E returned to the current sheet the first time at 52 R_E (41 R_E) and the second time at 45 R_E (32 R_E).

[17] The model result (Figure 1c) also indicates that the time it takes from the injection of the first ion structure (t = 0) to the encounter of the first echo (concave slope) is not simply z = 3x (x being the time interval from the injection to the first spacecraft encounter) as would be expected in a nonconvecting magnetotail (dashed line). Instead, the actual time interval, y, is shortened in comparison to z. Similarly, the lowest-energy ions in the cluster arrive much earlier for the echo in the convecting magnetotail, which results in a significantly shortened dispersion trace of the echo in comparison to the echo trace of the nonconvecting magnetotail (dashed lines in Figures 1a and 1b). These effects are even more pronounced in the case of an ion injection at much larger distances as shown in Figures 1d and 1e. In this second run, the injection location and the energy range of the initial ion structure are 149 R_E and 3–10 keV, respectively, and were again chosen to match the observations of the event (20 February 2002) presented in section 5.2. Because of the larger tail distance we have chosen a larger average convection speed, v_d, of 440 km/s. We first note that the dispersion slope of the echo is again concave but with the difference that the tangent associated with the most energetic ions is nearly parallel to the slope of the first ion structure (Figure 1e). As a result, the intercepts of these two slopes with the 1/v = 0 line are separated significantly (about 9 min). It also leads to a significant shortening of the travel distance of the echo (187 R_E instead of 447 R_E). These features could be falsely interpreted in observations as two separate ion injections (c.f. section 5.2). Second, we note that the time it takes the ions from their injection to the first encounter with the spacecraft is about 11 min. The first echo appeared at the spacecraft only about 12 min (y-x) after the arrival of the initial injection. This is significantly shorter than 22 min (z-x) which would be expected for an echo traveling in a nonconvecting magnetotail. This shows that the field lines shortened more during the longer ion travel times and under the increased convection speed compared to the first run (Figures 1b and 1c), and thus making an identification of BIC even more difficult for very far-tail (>100 R_E) ion injections. Again, we point out the extreme shortening of the echo trace caused by the tail convection (Figures 1d and 1e).

[18] In summary of this section, if the tail field lines were not convecting and no secondary neutral sheet acceleration

occurred, the travel distance ratios of an initial ion structure and two echoes would be 1:3:5, assuming the point of observation is much closer to the near-Earth reflection location than to the injection location in the magnetotail. The results of our kinematic model show that these ratios are not valid in the case of long ion travel times during which substantial field line shortening can occur. Therefore it is not possible to use the 1:3:5 ratio as an indicator for BIC of ion structures that were injected in the far tail PSBL (>50 R_E). The model also demonstrated two new features of BIC in 1/v versus time spectrograms: (1) concave dispersion slopes and (2) near-parallel dispersion slopes of initial ion injection and echoes. In spite of the fact that we have not included several other effects acting on the ions, this model helps in interpreting the observations of BIC events reported in section 5. In section 6.2 we will further discuss the scope and limitations of this model.

4. Determination of the Plasma Regions

[19] The most widely accepted division of plasma regions in the tail plasma sheet includes the PSBL and the central plasma sheet (CPS). The PSBL, located between the lobe and the CPS, is foremost defined by the presence of ion beams [*DeCoster and Frank*, 1979; *Eastman et al.*, 1984; *Takahashi and Hones*, 1988], although other signatures were later found to be frequently present in the PSBL as well. The CPS is characterized by more isotropic ion distributions, although ion beams can also occur in this region. To identify the plasma region in which the here reported ion beams occurred, criteria other than the presence of ion beams had to be considered. Often, the mean energy profile in the CPS increases monotonically toward lower L values due to adiabatic compression of the convecting CPS plasma. The start of this energy increase was used here as the indicator for the PSBL-CPS boundary. We note here, however, that a unique boundary between the PSBL and the CPS has not yet been established in the literature. In fact, it is also not clear whether one or several physical properties are required to define such a boundary.

[20] It should be pointed out that some studies [e.g., *Feldstein and Galperin*, 1994] have used the term boundary plasma sheet (BPS) to denote a region between the tail lobes and the CPS in the magnetotail. The authors make the case that the BPS is somewhat larger than the PSBL, including the low-energy particle layer reported by *Parks et al.* [1992]. This BPS, however, differs from the BPS at ionospheric altitudes as defined by *Winningham et al.* [1975]. On the basis of electron observations from low-altitude satellites, the nightside auroral zone field lines have been divided into the BPS and the CPS [*Winningham et al.*, 1975]. The distinguishing feature between the BPS and the CPS are structured and unstructured precipitation of electrons, respectively. In this scheme the BPS could be the low-altitude signature of the PSBL [*Eastman et al.*, 1984; *Newell et al.*, 1991]. However, the mapping of the CPS from low to high altitude is not simply a one-to-one mapping in the Winningham et al. definition [*Newell et al.*, 1991].

[21] The term PSBL applied to the magnetotail has received wider acceptance than BPS, and thus we will use this term here as the region that lies between the tail lobe and the CPS. The current understanding of the topology of the magnetosphere is such that PSBL field lines cross the current sheet in the far tail of the magnetosphere. The current sheet continues into the CPS but the field lines gradually become more dipolar. This has important consequences regarding the adiabaticity of particles traveling either on PSBL or CPS field lines, which will be discussed in section 6.3.

5. Event Studies

[22] We looked for BIC signatures in 95 PSBL crossings at geocentric distances of 4–6 R_E, while restricting the survey to the local time sector from 21 to 3 hours. Here we present three events that are of the same type in the sense that the ion injection region was located in the far tail (>39 R_E) and extended to the outer edge of the PSBL. All events occurred during the recovery phase or quiet times and are most likely associated with (not necessarily caused by) the far-tail X line. During several other PSBL crossings (<10) we found similar BIC signatures as reported here.

[23] In this section we will assume that the dominant effect causing the energy dispersion of the BIC is due to the time-of-flight effect. In section 6.1 we will justify this assumption. By making this assumption, we can determine the ion injection location using the 1/v-method as outlined in section 3.

5.1. Event 1: 14 February 2001

[24] During the PSBL crossing on 14 February 2001, Cluster encountered multiple energy-dispersed ion structures (Figure 2a). The first structure (labeled A) is located at the outer edge of the PSBL, or essentially defines this outer edge. Structures B and C are on lower L shells, i.e., deeper inside the plasma sheet. To determine the plasma region in which each dispersive ion trace occurred, we plotted the mean ion energy in Figure 2b. The vertical line indicates the beginning of a steady increase in energy which we identify as the PSBL-CPS boundary (see section 4). Therefore A and B are in the PSBL and C is located at the PSBL-CPS boundary. No additional ion structure can be seen in the CPS which is fairly isotropic. Substorm recovery phase prevailed during this PSBL crossing (Figure 3a) and geomagnetic activity was somewhat disturbed: Kp = 4-. At the same time, ultraviolet images from the IMAGE satellite show a double oval (Figures 3b and 3c) which is a typical recovery phase signature [*Elphinstone et al.*, 1995]. The footprints of the Cluster spacecraft, mapped into the Northern Hemisphere ionosphere, are indicated by a square. The Cluster spacecraft were also magnetically conjugate to a small activated region in the poleward arc of the double oval.

[25] This event has been investigated by *Keiling et al.* [2004a] where a comparison of the ion measurements from SC 1, SC 3, and SC 4, and a discussion of the fine structure (beamlets) of the dispersed ion structures can be found. Keiling et al. already pointed out that A, B, and C are BIC. However, here we improve their analysis of the BIC signatures. Figures 2c and 2d are expanded views, showing that the dispersed ion structures A, B, and C consist of substructures. Structure A shows three smaller-scale structures (labeled beamlet A1, A2, and A3). Similarly, structure B consists of three beamlets (B1, B2, B3) and structure C could possibly consist of two beamlets (C1, C2) which, however, is not certain. For the analysis that follows we

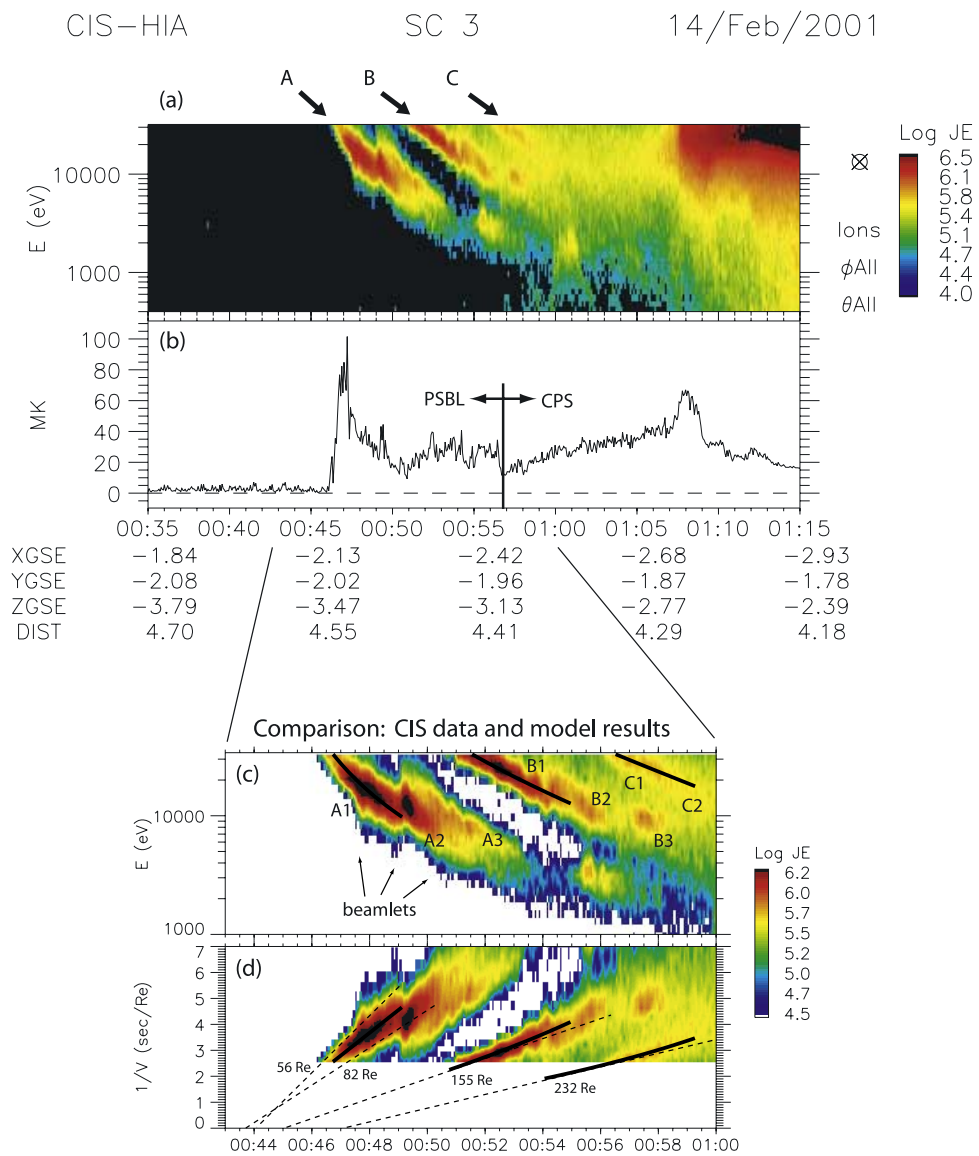

Figure 2. Comparison of CIS data from Cluster 3 and model results: (a) PSBL crossing on 14 February 2001 showing bouncing ion clusters (labeled A, B, C); (b) ion energies in units of Kelvin used to identify the PSBL and CPS; (c) and (d) expanded views of the bouncing ion clusters plus model results (black lines). Several beamlets can be seen. The values next to the dashed lines indicate travel distances.

treat the beamlets of A as independent ion injections following *Keiling et al.* [2004a] and associate B1 and C1 with A1, and B2 with A2. A comparison with the model results is first done for A1 and its echoes, followed by a comparison for A2 and its echo.

5.1.1. First Beamlet and Its Echoes

[26] Overlaid on Figures 2c and 2d are the model results (from Figures 1b and 1c). The input parameters to the model were the distance and the energy range of the initial ion injection, the speed of the earthward convection of tail field lines, and the secondary energization ratio (see section 3). The comparison shows that several observational features are reproduced by the model.

[27] First, we note the general trend that the dispersion slopes of corresponding beamlets (A1, B1, and C1) get shallower in both observations and model (black lines), which implies increased travel distances for B1 and C1 (Figures 2c and 2d). This is expected if these beamlets are in fact echoes. The values next to the slopes are the inverse of the slopes which indicate the travel distance in the case of time-dispersed ions (TDIS). For beamlet A1, both the leading and the trailing edges are indicated to show the range of injection distances consistent with the data. If we assume that the dispersion signatures are due to the time-of-flight effect, then the different slopes of the leading and trailing edges of structure A1 imply that the ions were impulsively injected during less than 30 s over an extended region ($\sim$26 R_E) in the magnetotail. The average travel distance associated with these two slopes is 68 R_E which is the distance used for the model calculation. A similar interpretation of leading and trailing edge has been given by *Kazama and Mukai* [2003] for their event.

[28] The beamlet B1 shows not only a shallower dispersion slope than A1 but also a concave dispersion slope in

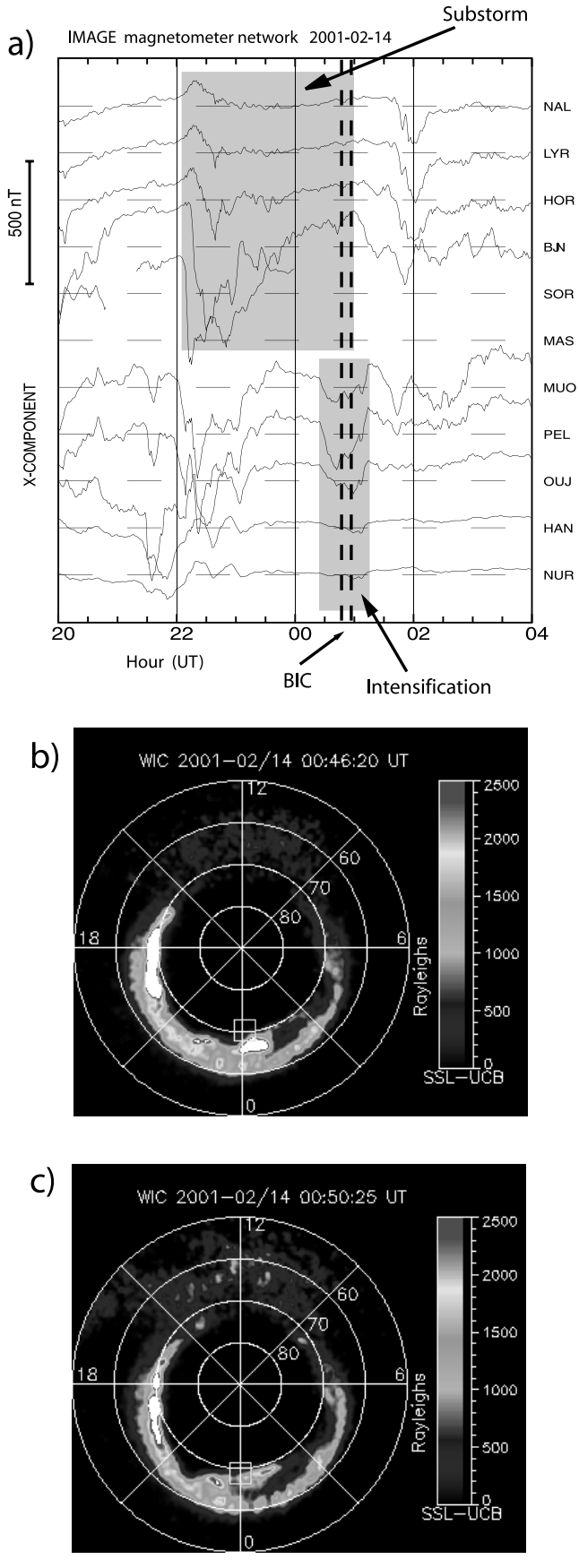

Figure 3. (a) Ground magnetometer data from IMAGE during the bouncing ion cluster (BIC) event on 14 February 2001. The grey areas indicate a substorm and intensification. Dashed lines mark the beginning and the end of the BIC recorded by Cluster. (b, c) Far-ultraviolet images from WIC on board the IMAGE spacecraft, showing a double oval in the Northern Hemisphere. Cluster's footprints (squares) were mapped using Tsyganenko T89.

the 1/v versus time spectrogram (Figure 2d). This feature is similar to the model calculation (black line), although slightly more pronounced. This concaveness was explained in the model by earthward convection of tail field lines, causing ions with different energies in the ion cluster to travel different distances (see section 3). As a further consequence, the extensions of the dispersion traces of A1 and B1 (dashed lines) do not intercept on the 1/v = 0 line but are separated by about 90 s.

[29] The second beamlet (C1) also shows a concave slope in the model (Figure 2d). It is unclear whether the data confirm this because the beamlet is less defined and is reduced in energy flux, making an identification of the dispersion slope more difficult.

[30] Furthermore, in the observational data the echo beamlets (B1 and C1) do not cover the same energy range as A1 anymore. B1 and C1 clearly exceed the upper threshold of the instrument (which is 34 keV) for high energy fluxes (red color), whereas A1 shows a smaller energy flux at the highest energies, indicated by the yellow color that surrounds the more intense (red) energy flux. Similarly, the lower energy ions of A1 are missing in both B1 and C1. One possible explanation is that all particles of A1 underwent additional acceleration when returning to the neutral sheet repeatedly. This would shift the entire population of the ion cluster to higher energies. This energy shift was reproduced in the model by energizing the ions on their return to the current sheet (see shift of the solid lines of the echo beamlets, Figures 2c and 2d).

[31] In summary, the ion observations are very similar to the model results, suggesting that B1 and C1 are the echoes of A1. This good agreement also supports our assumption of a time-of-flight effect for the dispersion since a time-of-flight effect was incorporated into the model.

5.1.2. Second Beamlet and Its Echoes

[32] In Figure 4a, model results (dashed lines) are shown for the second ion injection, A2, at 42 R_E about 2.5 min after the first injection, A1. The model results of beamlet A1 and its echoes are also included (solid lines). The model dispersion slopes (overlaid in Figures 4b and 4c) match the observations reasonably well to suggest that B2 is indeed the echo of A2. We note that the dispersion slope of B2 is less concave in the observation and not visible in the model results (Figure 4c). This is due to the closer injection distance (compared with A1) and the reduced convection speed in the tail, which was chosen to be 140 km/s. Note that this convection speed is smaller than the convection speeds that were applied for A1 (350 km/s) and B1 (180 km/s). Since A1 was injected at 68 R_E and B1 returned to the current sheet at 52 R_E, whereas A2 was injected at 42 R_E, these differences support the argument of an increasing convection speed with increasing distances from Earth (see

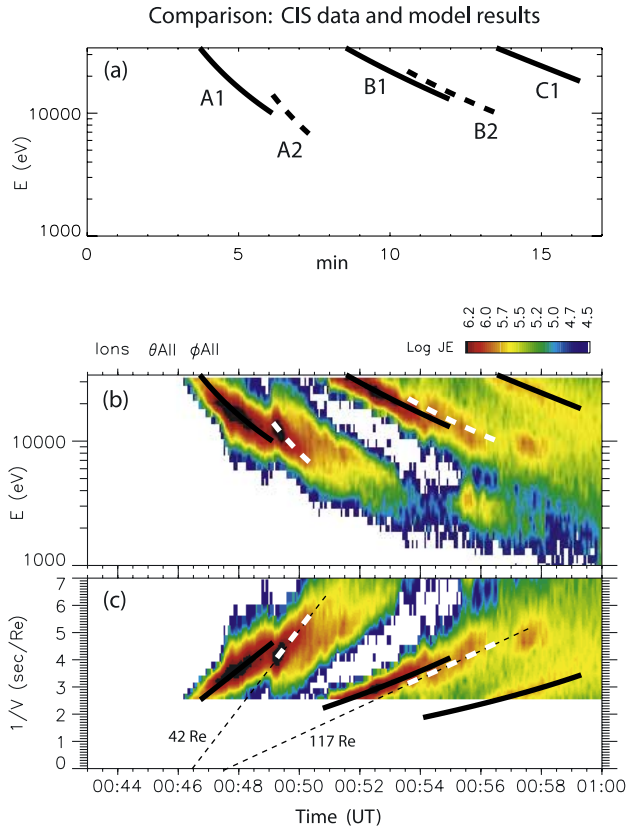

Figure 4. Comparison of CIS data from Cluster 3 and model results: (a) Model results of the first (solid lines) and the second (dashed lines) ion injections and their echoes in comparison to (b, c) the observations from Cluster 3 on 14 February 2001.

section 3). Similar to the echo of A1, the echo of A2 shows higher energies which were accounted for in the model by a secondary acceleration in the magnetotail (see section 3).

[33] A second echo of A2 is not clearly visible in the measurements. The lower energy flux of B2 compared with A2 might have been effectively thermalized after the third interaction with the current sheet. This same fate most likely happened to C1 at its fourth interaction with the current sheet. In general, one can note that the energy fluxes of subsequent echo beamlets were increasingly reduced. This suggests that the echoes became increasingly thermalized during successive current sheet encounters until they mixed entirely with the isotropic ion population of the CPS. Another loss mechanism is partial precipitation into the ionosphere. Note that we have not modeled beamlet A3 (Figure 2c) because it is too faint and shows no obvious echo.

5.2. Event 2: 20 February 2002

[34] The second example of BIC presented here occurred on 20 February 2002 during geomagnetic quiet times (Kp = 1-). UV images from IMAGE were not available for this event. Two energy dispersion traces (labeled A and B) were recorded in the PSBL (Figures 5a and 5b). Their peak energies were below the instrument's upper threshold (<34 keV) which is also indicative of the very quiet time. The ion energy range was about 3–10 keV. As for Event 1 (but less pronounced), the high-energy cutoff of B was slightly higher than that of A.

[35] Expanded views are shown in Figures 5c and 5d, overlaid by the model results of ion injections at 149 R_E with an earthward convection speed of tail field lines of 440 km/s (see section 3). The model dispersion slopes (black lines) line up reasonably well with the observed dispersion slopes, suggesting that B could be the echo of A. Note that because B shows less energy flux and its structure is less defined, it is not possible to accurately identify its dispersion slope. The less-defined boundaries of this ion structure might also account for the lack of visible slope concaveness which is present in the model (Figure 5d) and which was also present in the observed echo of Event 1.

[36] The first structure A displays a leading edge and a trailing edge with different slopes which is similar to Event 1 (Figure 5d). Assuming an impulsive injection, leading and trailing edge yield travel distances of about 129 and 169 R_E, suggesting a broad injection region of about 40 R_E. These large distances are consistent with the prevailing quiet time which could result in a distant X line. All particles were approximately injected within 2 min around 0438 UT. The most energetic ions took about 11 min to reach the spacecraft and the lowest-energy ions took about 20 min. The second structure B was encountered about 12 min after the encounter of A. This delay is significantly shorter than would be expected for an echo in a magnetotail without convection, as shown by the model results in section 3 (dashed black line in Figure 1e). However, model calculations show that an ion injection at 149 R_E (which is the average distance of the leading and trailing edge of A) and an average earthward convection speed of 440 km/s reproduce this shortened time delay (Figures 1d and 1e).

[37] Another critical observation is that the dispersion slope of echo B is nearly parallel to the one of A (Figures 5c and 5d), and, consequently, their extension lines (dashed lines) do not intercept on the 1/v = 0 line. In contrast, for Event 1 the dispersion slopes got progressively shallower with each echo. According to the model results, this difference between Event 1 and Event 3 results from a much larger injection distance and a larger convection speed for Event 3. Without the model, the near-parallel dispersion slopes of A and B could falsely lead to the conclusion that B is an independent ion injection. Instead, we find it very likely that B is indeed the echo of A. Further support comes from a significant reduction of energy flux for B compared with A, which again suggests that the echo underwent some scattering/thermalization during the second interaction with the current sheet (c.f. Event 1).

5.3. Event 3: 5 February 2002

[38] The last BIC event presented here was chosen because it shows possibly up to three echoes of an ion cluster injected into the outer edge of the far-tail PSBL (labeled A, B, C, and D in Figure 6a). It also shows that ion clusters can bounce long enough for convection to carry them into the CPS. From the mean energy plot (Figure 6b), we identify the PSBL-CPS boundary to be crossed by the spacecraft at about 2312 UT (see section 4), which places two echoes (C and D) inside the CPS. Note that an additional dispersion trace is present between A and B which will not be further considered here. This event

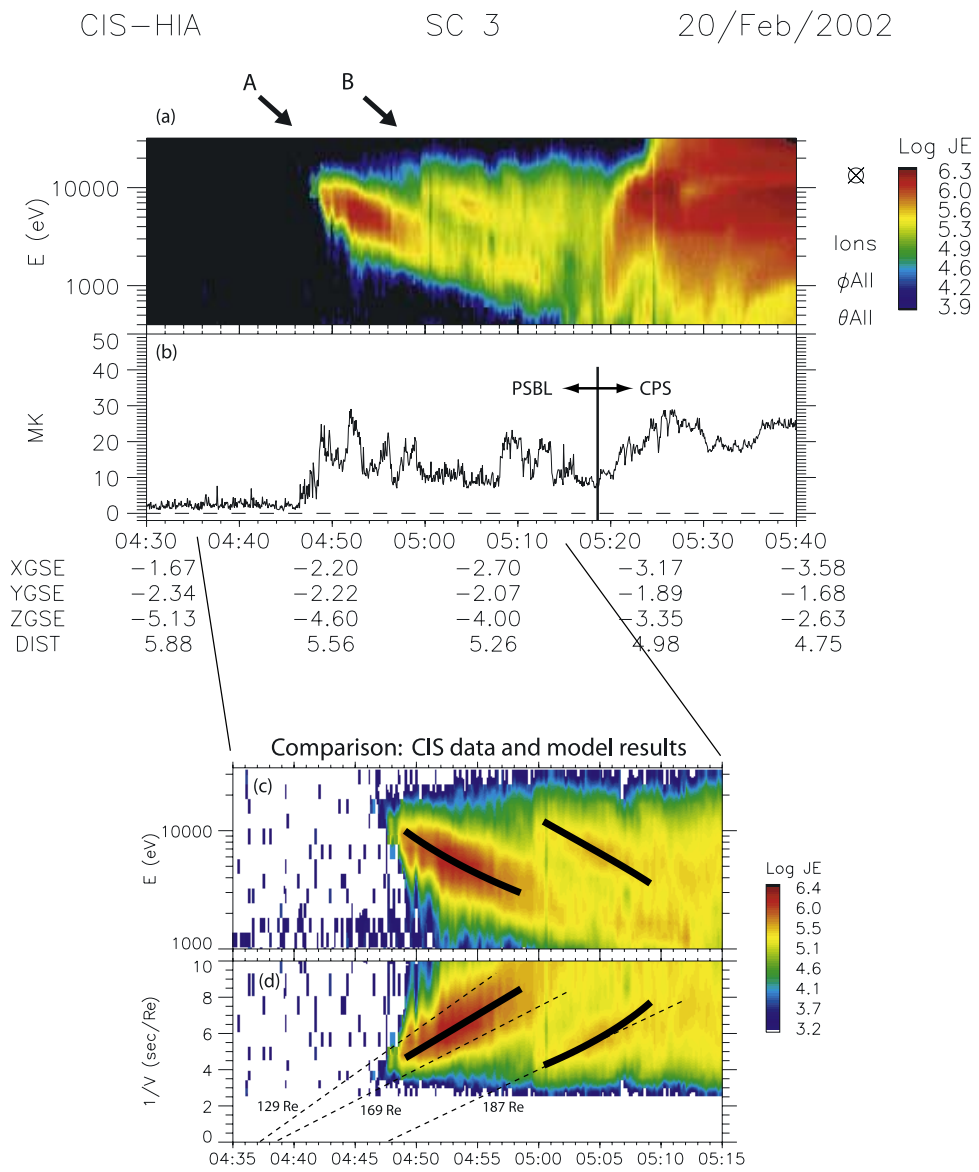

Figure 5. Comparison of CIS data from Cluster 3 and model results for the PSBL crossing on 20 February 2002 during which bouncing ion clusters were recorded (labeled A and B). Same format as Figure 2.

occurred during a substorm recovery phase (Figure 7a) with elevated Kp = 5-. UV images closest to the time of the BIC are shown in Figures 7b and 7c. A double oval is visible, and thus it is likely that Cluster might have been magnetically conjugate to the poleward arc of the double oval similar to Event 1.

[39] In the expanded plots (Figures 6c and 6d), the structure A shows several up- and down-steps which makes it more difficult to identify one slope line. As for the previous two events, structure A shows a leading and a trailing edge, suggesting travel distances of 39 and 71 R_E (Figure 6d). Leading and trailing edge roughly intercept at the same point on the 1/v = 0 line.

[40] The second and third echoes (C and D) show large flux reductions and less defined dispersion traces which is similar to the later echoes of the previous two events. This event thus is another example of the scattering/thermalization process in the current sheet acting on ion beams to the extent that they eventually contribute to the isotropic CPS plasma.

[41] The model results are overlaid (black lines) and delineate the observed ion structures, in particular for A and B (Figures 6c and 6d). The observed traces of the second (C) and third (D) echo are poorly defined so that a direct comparison to the model slopes is not possible. However, it can be noted that there is good agreement in the locations of the modeled slopes and the observed ion structures.

[42] This event is more similar to Event 1 than Event 2 in terms of injection distance, energy range, and geomagnetic activity. However, we note that the concaveness in the dispersion slope of echo B (as was present for Event 1) is not visible in the CIS data (Figure 6d). The lack of discernable concaveness was achieved in the model by reducing the convection speed to values of the order of

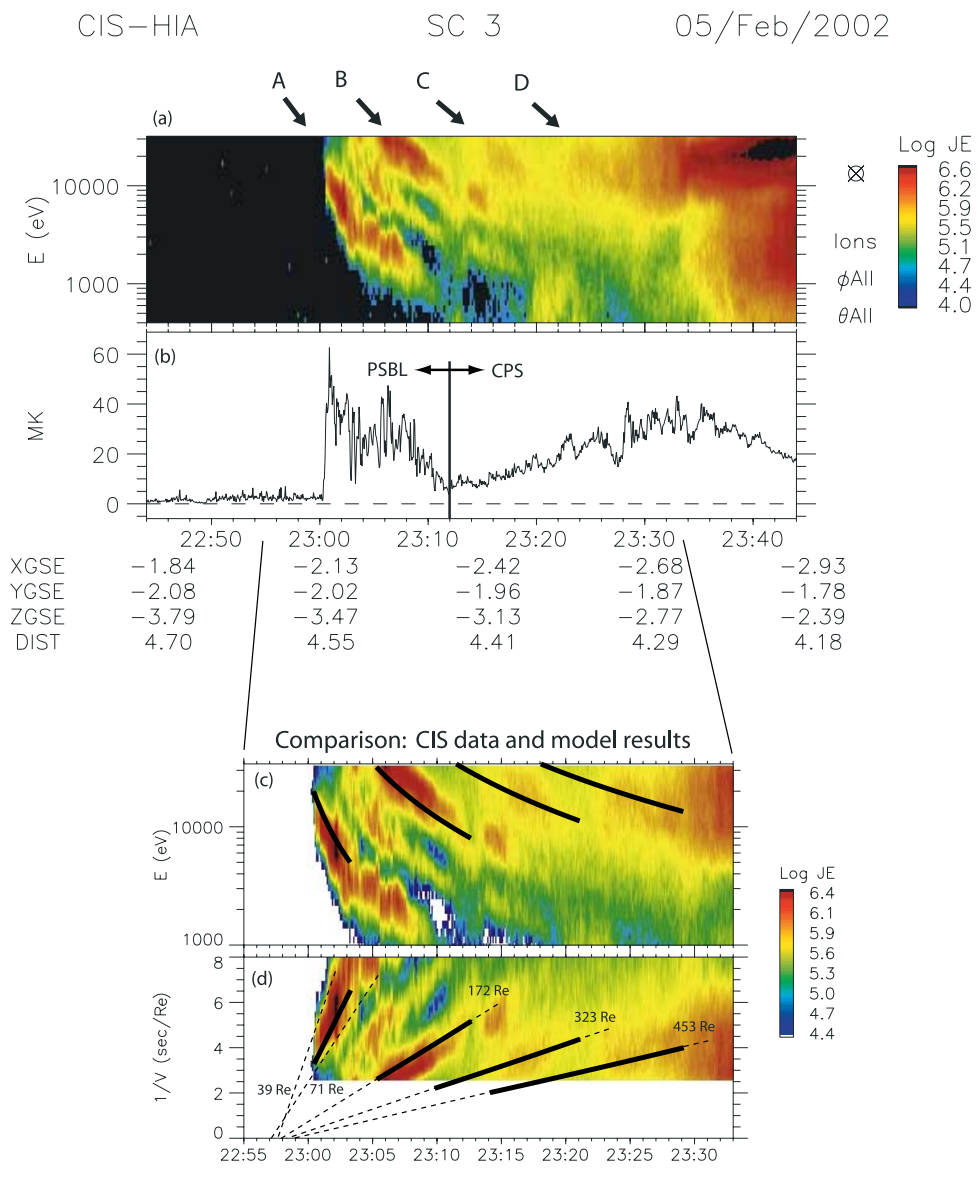

Figure 6. Comparison of CIS data from Cluster 3 and model results for the PSBL crossing on 5 February 2002 during which bouncing ion clusters were recorded (labeled A, B, C, and D). Same format as Figure 2.

40 km/s. One justification for a smaller speed is the closer injection distance compared with Event 1, which agrees with observations that the convection speeds are smaller closer to Earth [*Paterson et al.*, 1998]. However, it is still possible that this speed was chosen too small and other unaccounted effects played a role as well. Also, compare the echo B2 of this event with the echo of the beamlet A2 of Event 1 (Figure 4c). There it was shown that because of a closer injection distance and reduced convection speed, little to no concaveness was present. For the same reason, the slopes of the modeled echoes C and D (black lines in Figure 6d) show no discernable concaveness.

[43] Another notable difference is the much lower upper energy (about 20 keV) of structure A compared with B. The energy difference appears to be much larger than 14 keV and it is questionable whether this can be attributed to the secondary neutral sheet acceleration of the echo alone (as was done for Event 1). A possible explanation could be that the initial ion structure A was injected with similar energies as A of Event 1, but because of its transient nature (as suggested by the common focus of the leading and trailing edges), ions with energies greater than 20 keV were simply missed by the spacecraft because they might have had already passed as the spacecraft entered the PSBL.

6. Discussion

[44] The problem of identifying BIC injected from the far-distant magnetotail is intrinsically difficult because of long ion travel times, a changing magnetotail during these times, and our limitation with the present satellites to monitor the tail properties, such as earthward convection, over large distances and over long time periods. Currently, one has to rely on sparse, local measurements of the

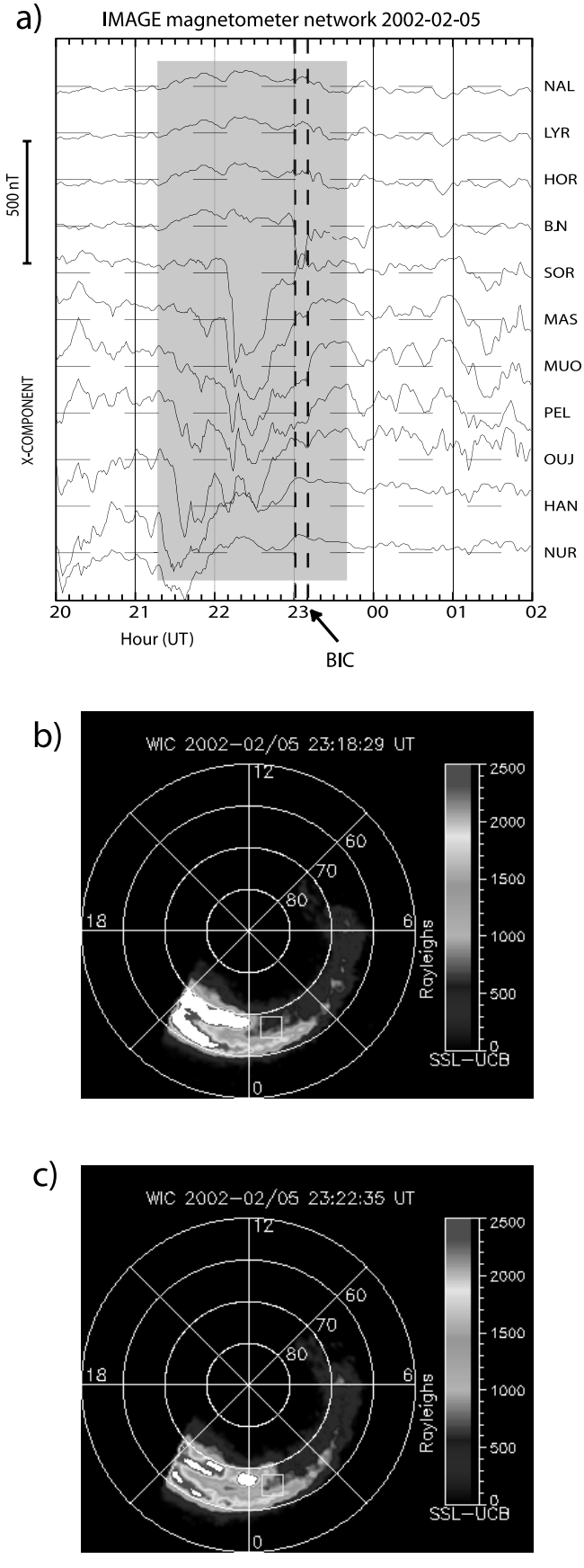

Figure 7. (a) Ground magnetometer data from IMAGE during the bouncing ion cluster (BIC) event on 5 February 2002. The grey area indicates a substorm. Dashed lines mark the beginning and the end of the BIC recorded by Cluster. (b, c) Far-ultraviolet images from WIC onboard the IMAGE spacecraft, showing a double oval in the Northern Hemisphere. Cluster's footprints (squares) were mapped using Tsyganenko T89.

physical properties of the magnetotail. In spite of these difficulties, we presented three PSBL crossings that showed multiple energy-dispersed ion structures which we identified as BIC with the aid of model calculations. On the basis of the time-of-flight effect, the injection regions were estimated to be greater than 39 R_E and up to 169 R_E.

[45] Support for the BIC scenario came also from the Cluster observations that the secondary structures (echoes) showed reduced energy fluxes but at higher energies compared with the initial ion injection. These two features can be attributed to scattering processes and neutral sheet acceleration during additional current sheet interactions of returning echoes [*Ashour-Abdalla et al.*, 1992]. If the multiple dispersed ion structures were new ion injections, one might expect similar intensities for all dispersion traces.

[46] It should be emphasized that the term "echo," used in this study to describe the multiple dispersed ion structures, is not intended to imply that all ions of structure A returned to the spacecraft location to form the echo structures B, C, etc. This is in fact very unlikely considering the large travel distances of over 300 R_E for echoes. Instead, we suggest that A has an azimuthal and longitudinal spread that is larger than observed at Cluster and thus the term "echo" refers to any ions that were part of this initial larger ion cluster.

[47] In the following subsections we will further discuss the cause of the dispersion effect in BIC, our model assumptions and limitations, the nonadiabatic conditions in the far-tail PSBL, and possible injection mechanisms.

6.1. Dispersion Effect

[48] The three BIC events were observed on inbound crossings of the PSBL in the local time sector from 0 to 3 hours. The interpretation of the cause of the associated energy dispersion (time-of-flight effect or velocity-filter effect) was thus complicated by the fact that the PSBL was crossed from the southern lobe toward the equatorial plane, which is in the same direction as the presumed $\mathbf{E} \times \mathbf{B}$ drift motion of the ambient plasma. This means that the observed decline in ion energy of each dispersive ion structure is both a decline with decreasing latitude, as would be expected with VDIS, and a decline over time, as would be expected with TDIS.

[49] On the basis of the following arguments, however, we suggest that the energy dispersion of the BIC events were dominated by the time-of-flight effect. First, because we did not find BIC that started at the outer edge of the PSBL during outbound crossings, that is when the spacecraft travels against the presumed large-scale plasma convection, it might be that it is impossible to record BIC in the PSBL during outbound crossing. If this is the case, then spatial energy dispersion can be ruled out for the BIC because the direction of the spacecraft motion should not play a major role in the detection process. On the other

hand, time-dispersed ion structures also undergo $\mathbf{E} \times \mathbf{B}$ drift, and thus a spacecraft traveling against this drift is very unlikely to see a possible echo (and even less likely to see three echoes as observed) for time-dispersed BIC. Hence on the basis of our generalization, we tentatively conclude that a time-of-flight effect caused the energy dispersion that allowed us to identify BIC. We note, however, that since Cluster traveled with 4–5 km/s perpendicular to magnetic field lines during the BIC events, the convection of the ambient plasma probably played a role in facilitating the recording of the BIC.

[50] Second, all events showed a leading and a trailing edge with different slopes intercepting the $1/v = 0$ line in close temporal proximity. This argues for a short-lived injection from a broader region in the magnetotail.

[51] Third, the observations, in particular the new feature of concave dispersion slopes (see also section 6.2), were in good agreement with the model results. The model was based on an impulsive injection scenario.

[52] The temporal interpretation is also in accordance with the results of a Polar-spacecraft-based survey [*Lennartsson et al.*, 2001] in which both inbound and outbound crossings of the PSBL were considered at 4–7 R_E. It was argued that the PSBL only supports TDIS (no BIC were however reported). Further, a recent Cluster study also showed evidence of TDIS in the PSBL during an outbound crossing [*Keiling et al.*, 2004b].

6.2. Model Assumptions, Limitations, and Results

[53] A kinematic model was used to verify that the multiple energy-dispersed ion structures observed in the PSBL are consistent with echoes of an initial injection in the far magnetotail. The four important features of this model were (1) impulsive ion injection in the far magnetotail; (2) broad energy range of injected ions; (3) earthward convection of magnetic field lines; (4) secondary acceleration of ions on returning to the current sheet. These few assumptions reproduced the observations well. However, we cannot rule out that other effects might also have played a significant role in the ion motion as outlined next.

[54] The ions that are nonadiabatically accelerated in the far tail (>39 R_E) become adiabatic as they approach the ionosphere. After mirroring in the converging Earth magnetic field, they return to the current sheet, where they again become nonadiabatic (and possibly chaotic) as will be shown in the next section. Hence the ions will interact in complex ways with the current sheet which includes scattering and additional acceleration [e.g., *Sergeev et al.*, 1983; *Ashour-Abdalla et al.*, 1992, 1993; *Delcourt et al.*, 1996]. This complex interaction has not been modeled here. Instead, we have ad hoc incorporated energization of each echo on each return to the current sheet. Our justification for doing so was based on the observations that the secondary structures (i.e., echoes) showed increased energies.

[55] It is well-known that the convective flow in the magnetotail varies with distance, geomagnetic activity, and during the cause of large-scale phenomena such as substorms. Generally speaking, it is impossible to monitor this flow over extended time periods and distances. Our approach was therefore to assume average velocities of the convective flows for the time periods between individual spacecraft encounters with dispersed ion structures.

[56] Furthermore, we have not included a realistic reflection of ions below the spacecraft by including the mirror force dependence on different pitch angles and possible parallel electric fields below the spacecraft.

[57] In spite of the model limitations, the simple model facilitated the identification of BIC events in the PSBL. In fact, our simple model could account for a new feature (concave dispersion traces) in the observations. This feature is mostly determined by the geometric parameters rather than the nonadiabatic motion of the ions in the current sheet. Furthermore, our model could account for (1) variations in the dispersion slope ratios that deviate from the 1:3:5 ratios and (2) for the lack of a common intercept of BIC dispersion slopes in 1/v spectrograms. These are two properties that are commonly used as identifiers for BIC in the CPS [*Hirahara et al.*, 1996].

6.3. Nonadiabaticity

[58] The ion injections occurred into the PSBL, and it was shown that subsequent echoes continued to be on PSBL field lines. In one event, due to the large-scale tail convection, later echoes were also observed on CPS field lines. The identification of echoes in the PSBL is important because PSBL field lines cross the current sheet in the far tail where nonadiabatic and stochastic motion is important, leading to the acceleration and scattering of ions [*Speiser*, 1964; *Sergeev et al.*, 1983]. Theoretical studies have identified the importance of the curvature parameter, κ, for particle motion in the magnetotail [e.g., *Büchner and Zelenyi*, 1989]. This parameter is defined as the square root of the ratio of the minimum magnetic field curvature radius to the maximum Larmor radius of the particle. Generally, it is assumed that ions with $\kappa \gg 1$ (<1) behave adiabatically (nonadiabatically). At $\kappa \sim 1$, the particles are in the chaotic regime. Some studies [*Sergeev et al.*, 1983; *Delcourt et al.*, 1996] have placed the transition between adiabatic and nonadiabatic conditions at $\kappa^2 = 8$.

[59] Now we give estimates of κ for some of the ions comprising the BIC events reported here. First, we note that due to the large-scale convection of magnetotail plasma during the travel time of the ions, the echoes returned to the equatorial plane at distances nearer to Earth than the initial injection sites. For Event 1, we estimated, using our model calculations, that ions injected with a range of energy (10–34 keV) at 68 R_E returned to the current sheet between 41 R_E (for 10-keV ions) and 52 R_E (for 34-keV ions). This range can be explained with the fact that the tail field lines had more time to convect earthward for slower particles.

[60] To calculate κ, we need to know the magnitude of the normal magnetic field component and the curvature radius of the magnetic field at the point where the echo encountered the field reversal region in the current sheet. These values could not be measured directly in the magnetotail for our event. Instead we use statistical data from previous studies. For 41 R_E and 52 R_E, we use 2.7 nT and 2 nT for the normal magnetic field component, respectively [*Slavin et al.*, 1985]. To estimate the minimum curvature radius, we use the study by *Shen et al.* [2003], where it was shown that the radius varies with substorm phases. During recovery phase the radius is largest and can be 2 R_E. Since this phase corresponds to our event, we use 2 R_E for the minimum curvature radius. Using these values for Event 1, we obtain $\kappa = 1.54$ (at

41 R_E) and $\kappa = 0.98$ (at 52 R_E) for 10 keV and 34 keV ions, respectively. For both cases, the values show that the ions are in the nonadiabatic regime and possibly in the chaotic regime. The nonadiabatic conditions during the BIC events separate them from those BIC that are routinely observed at geosynchronous orbit [e.g., *Quinn and McIlwain*, 1979]. These BIC experience little particle flux reduction because they travel on more dipolar field lines where the particle motion is adiabatic. Unless other disturbances are present, these adiabatic BIC can survive many bounces even during the substorm expansion phase. Considering that the ions of the BIC presented here are in the nonadiabatic regime and even close to the chaotic regime, it is surprising that the ion cluster can be sustained for several bounces and for total travel distances greater than 200 R_E.

[61] Two important additional features of the echoes were observed which also support the nonadiabatic BIC interpretation: (1) Subsequent echoes had higher energies compared to the initial ion beams which can be attributed to the secondary nonadiabatic acceleration in the current sheet during their repeated interactions with the current sheet. (2) The echo energy fluxes were reduced and the echoes became more diffuse. This was possibly caused by the gradual thermalization during consecutive current sheet interactions and by partial precipitation into the ionosphere. Both particle signatures have been produced in kinetic simulations of ion trajectories in the magnetotail [*Ashour-Abdalla et al.*, 1992, 1993]. Furthermore, *Sergeev et al.* [1983] showed that in the nonadiabatic regime scattering preferentially occurs into the loss cone. This effect would also explain the energy flux reduction in the echoes that we reported.

6.4. Generation Mechanism of BIC

[62] The injection locations of the BIC events reported here, determined on the basis of the TOF interpretation, ranged from 39 to 169 R_E. Using ISEE 1 and 2 data, *Williams* [1981] showed ion beams in the PSBL coming from regions in the magnetotail at 80 to 100 R_E. Later, *Takahashi and Hones* [1988] did a comprehensive study on ion beams in the PSBL and showed a specific ion velocity profile with higher velocities closer to the lobe-PSBL interface. These studies did not report BIC signatures. However, our events are most likely of the same origin in the distant magnetotail. Therefore the BIC reported here must be distinguished from those reported in the CPS at distances less than 30 R_E [e.g., *Quinn and McIlwain*, 1979; *Hirahara et al.*, 1996] where the plasma conditions are vastly different from those in the far tail (Figure 8). At geosynchronous distances, BIC are routinely observed because κ is in the adiabatic regime and the plasma beta is much less, providing more stable conditions for ion beams. There appears to be consensus that the adiabatic BIC are generated by the convection surge mechanism [*Quinn and Southwood*, 1982]. Observations and simulations support this mechanism [*Mauk*, 1986]. This mechanism is based on dipolarization and has been used as an injection mechanism up to 30 R_E geocentric distance in the magnetotail [*Hirahara et al.*, 1996; *Kazama and Mukai*, 2003]. Since our BIC are injected much further out in the tail, it is unlikely that dipolarization was the injection cause.

[63] The initial ion formation of the BIC events reported here occurred at the outer edge of the PSBL. With the current understanding of the magnetotail topology, this implies that the ions were ejected near the reconnection region in which open field lines are reconnected to form closed field lines. Furthemore, the initial ion structures showed a leading and a trailing edge with different slopes, which argued for a broad injection region (up to 40 R_E). Such distributed sources are discussed by *Zelenyi et al.* [1990] and are associated with neutral sheet acceleration. Neutral sheet acceleration has also been invoked by *Ashour-Abdalla et al.* [1992, 1993] who predicted BIC in the PSBL. However, Ashour-Abdalla et al. assumed quasi-static injections in contrast to our transient injection scenario.

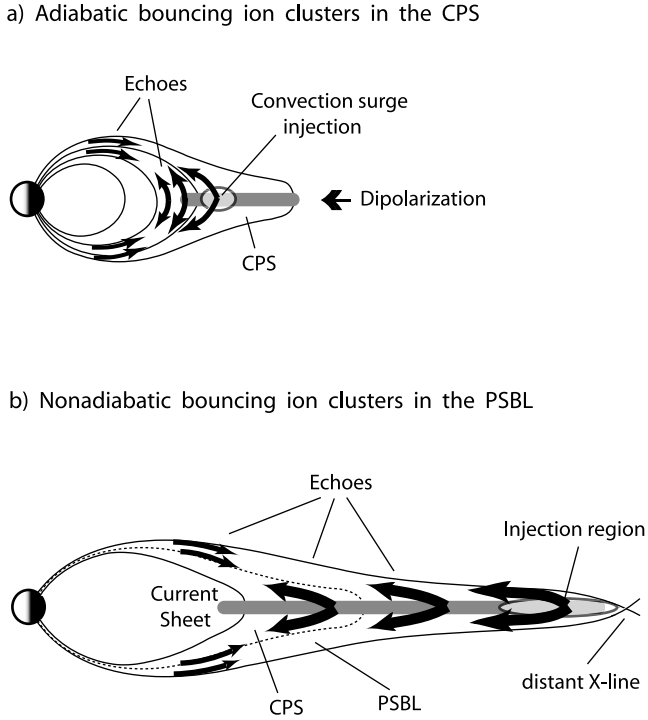

Figure 8. Two types of bouncing ion clusters (BIC). (a) Adiabatic BIC in the CPS injected at distances less than 30 R_E (adapted from *Hirahara et al.* [1996]). (b) Nonadiabatic BIC in the PSBL injected in the distant magnetotail (>30 R_E). The dotted line depicts a possible CPS-PSBL interface. Echoes can at times (see Event 3) last until they are convected into the CPS. Note that only one extended injection region is depicted; however, additional injection regions can exist (see Event 1).

[64] It is important to note that during one PSBL crossing (Event 1) at least two separate BICs were recorded. An apparent larger-scale ion structure was substructured into several ion beamlets, each of which was interpreted as an independent injection, following *Keiling et al.* [2004a, 2004b]. These two studies proposed several scenarios to explain the beamlet substructure, one of which was that the ion beamlets were impulsively injected from multiple source islands with varying distances in the far-tail current sheet. This scenario is consistent with our calculations (using the time-of-flight effect) which show that each ion beamlet traveled different distances.

[65] It is possible that the BIC reported here are the high-altitude signatures of the BIC reported by *Bosqued et al.*

[1993]. These BIC were observed in the auroral zone (<2000 km) at the poleward edge of the auroral oval, and the authors argued that these field lines map to the PSBL. The energies of the ions ranged from several keV to tens of keV which is comparable to the energy range of the BIC reported here. However, *Bosqued et al.* [1993] argued that the observed BIC had a quasi-static source which is in contrast to our interpretation of transient injections. Of further interest is that their BIC events also occurred during the recovery phase of substorms, which is similar to our results. (We reported two BIC during the recovery and one BIC during quiet times.) This suggests, although it needs to be confirmed by additional observations, that BIC in the PSBL are associated with or most easily identified during this particular phase of the magnetotail. In the classic substorm picture [*Hones*, 1980], a near-Earth neutral line retreats during recovery to form the new distant neutral line. The BIC reported here occurred during this transition and possibly continued to occur after the distant neutral line was established.

7. Conclusions

[66] The important result reported here is the existence of nonadiabatic BIC in the PSBL that were associated with injections in the far tail (up to 169 R_E) as opposed to the adiabatic BIC which are associated with injections at much closer distances (<30 R_E) and which are commonly reported (see references in section 1). For BIC to exist, the prevailing opinion was that not only a stable magnetotail must prevail but also adiabatic conditions. Our observations show that BIC are also possible in the nonadiabatic regime and they therefore add to our understanding of plasma sheet dynamics (Figure 8).

[67] The ion injections associated with the nonadiabatic BIC are very likely of the same kind as the ion beams regularly recorded in the PSBL [*Eastman et al.*, 1984; *Parks et al.*, 1984; *Takahashi and Hones*, 1988]. Although these PSBL ion beams are very common, BIC observations are not. This however does not rule out that BIC are much more common than actually observed. The main difficulty is their detection which is only possible with a coherent energy dispersion signature. This signature, however, is most likely very vulnerable to perturbations in the magnetotail such as bursty bulk flow, MHD waves, and wave-particle interaction, and thus many BIC probably remain undetected. It appears that one favorable condition for BIC detection is that the magnetotail is in recovery or quiet phase.

[68] In interpreting the observations, we used a kinematic model which reproduced well several observational features (including new features). It also clearly demonstrated that when an earthward convection (due to $\mathbf{E} \times \mathbf{B}$) is included, the dispersion slopes of BIC are changed significantly for far-tail injections. This makes it impossible to use the ratio 1:3:5:etc. of travel distances to infer BIC for far-tail injections.

[69] **Acknowledgments.** The work at the University of California, Berkeley, was supported by NASA grants NNG04GF23G and NAG-11416. We also thank Ari Viljanen from the Finnish Meteorological Institute for the IMAGE ground magnetometer data. We thank the World Data Center for Geomagnetism at Kyoto, Japan, for providing the AE index. We also thank the reviewers for their critical comments.

[70] Lou-Chuang Lee thanks Craig A. Kletzing and another reviewer for their assistance in evaluating this paper.

References

Ashour-Abdalla, M., et al. (1992), Precipitation of fast ion beams from the plasma sheet boundary layer, *Geophys. Res. Lett.*, *19*, 617.

Ashour-Abdalla, M., et al. (1993), Shaping of the magnetotail from the mantle: Global and local structuring, *J. Geophys. Res.*, *98*, 5651.

Bosqued, J. M., et al. (1993), Dispersed ion structures at the poleward edge of the auroral oval: Low-altitude observations and numerical modeling, *J. Geophys. Res.*, *98*, 19,181.

Büchner, J., and L. M. Zelenyi (1989), Regular and chaotic charged particle motion in magnetotail-like field reversal: 1. Basic theory of trapped motion, *J. Geophys. Res.*, *94*, 1821.

DeCoster, R. J., and L. A. Frank (1979), Observations pertaining to the dynamics of the plasma sheet, *J. Geophys. Res.*, *84*, 5099.

Delcourt, D. C., et al. (1996), On the nonadiabatic precipitation of ions from the near-Earth plasma sheet, *J. Geophys. Res.*, *101*, 17,409.

Eastman, T. E., L. A. Frank, W. K. Peterson, and W. Lennartsson (1984), The plasma sheet boundary layer, *J. Geophys. Res.*, *89*, 1553.

Elphinstone, R. D., et al. (1995), The double oval UV auroral distribution: 2. The most poleward arc system and the dynamics of the magnetotail, *J. Geophys. Res.*, *100*, 12,093.

Feldstein, Y. I., and Y. I. Galperin (1994), Comment on "Low-energy particle layer outside the plasma sheet boundary" by G. K. Parks et al., *J. Geophys. Res.*, *99*, 13,537.

Hirahara, M., et al. (1996), Two types of ion energy dispersions observed in the nightside auroral regions during geomagnetically disturbed periods, *J. Geophys. Res.*, *101*, 7749.

Hones, E. W., Jr. (1980), Plasma flow in the magnetotail and its implications for substorm theories, in *Dynamics of the Magnetosphere*, edited by S. I. Akasofu, p. 545, Springer, New York.

Kazama, Y., and M. Mukai (2003), Multiple energy-dispersed ion signatures in the near-Earth magnetotail: Geotail observation, *Geophys. Res. Lett.*, *30*(7), 1384, doi:10.1029/2002GL016637.

Keiling, A., et al. (2004a), New properties of energy-dispersed ions in the plasma sheet boundary layer observed by Cluster, *J. Geophys. Res.*, *109*, A05215, doi:10.1029/2003JA010277.

Keiling, A., et al. (2004b), Transient ion beamlet injections into spatially separated PSBL flux tubes observed by Cluster-CIS, *Geophys. Res. Lett.*, *31*, L12804, doi:10.1029/2004GL020192.

Lennartsson, O. W., et al. (2001), Polar/Toroidal Imaging Mass-Angle Spectrograph survey of earthward field-aligned proton flows from the near-midnight tail, *J. Geophys. Res.*, *106*, 5859.

Mauk, B. H. (1986), Quantitative modeling of the "Convection Surge" mechanism of ion acceleration, *J. Geophys. Res.*, *91*, 13,423.

Mende, S. B., et al. (2000), Far ultraviolet imaging from the IMAGE spacecraft, 2, wide band FUV imaging, *Space Sci. Rev.*, *91*, 271.

Newell, P. T., et al. (1991), The low-latitude boundary layer and the boundary plasma sheet at low altitude: Prenoon precipitation regions and convection reversal boundaries, *J. Geophys. Res.*, *96*, 21,013.

Parks, G. K., et al. (1984), Particle and field characteristics of the high-latitude plasma sheet boundary layer, *J. Geophys. Res.*, *89*, 8885.

Parks, G. K., et al. (1992), Low-energy particle layer outside the plasma sheet boundary, *J. Geophys. Res.*, *97*, 2943.

Paterson, W. R., et al. (1998), Geotail survey of ion flow in the plasma sheet: Observations between 10 and 50 R_E, *J. Geophys. Res.*, *103*, 11,811.

Quinn, J. M., and C. E. McIlwain (1979), Bouncing ion clusters in the Earth's magnetosphere, *J. Geophys. Res.*, *84*, 7365.

Quinn, J. M., and D. J. Southwood (1982), Observations of parallel ion energization in the equatorial region, *J. Geophys. Res.*, *87*, 10,536.

Rème, H., et al. (2001), First multispacecraft ion measurements in and near the Earth's magnetosphere with the identical Cluster ion spectrometry (CIS) instrument, *Ann. Geophys.*, *19*, 1.

Sergeev, V. A., et al. (1983), Pitch-angle scattering of energetic protons in the magnetotail current sheet as the domination source of their isotropic precipitation into the nightside ionosphere, *Planet. Space Sci.*, *31*, 1147.

Shen, C., et al. (2003), Analyses on the geometrical structure of magnetic field in the current sheet based on Cluster measurements, *J. Geophys. Res.*, *108*(A5), 1168, doi:10.1029/2002JA009612.

Slavin, J. A., et al. (1985), An ISEE 3 study of average and substorm conditions in the distant magnetotail, *Geophys. Res. Lett.*, *90*, 10,875.

Speiser, T. W. (1967), Particle trajectories in model current sheets: 2. Applications to auroras using a geomagnetic tail model, *J. Geophys. Res.*, *72*, 3919.

Takahashi, K., and E. W. Hones Jr. (1988), ISEE 1 and 2 observations of ion distributions at the plasma sheet-tail lobe boundary, *J. Geophys. Res.*, *93*, 8558.

Williams, D. (1981), Energetic ion beams at the edge of the plasma sheet: ISEE 1 observations plus a simple explanatory model, *J. Geophys. Res.*, *86*, 5507.

Winningham, J. D., et al. (1975), The latitudinal morphology of 10 eV and 10 keV electron fluxes during magnetically quiet and disturbed times in the 2100–0300 MLT sector, *J. Geophys. Res.*, *80*, 3148.

Zelenyi, L. M., R. A. Kovrazhkin, and J. M. Bosqued (1990), Velocity-dispersed ion beams in the nightside auroral zone: AUREOL 3 observations, *J. Geophys. Res.*, *95*, 12,119.

E. Amata, Instituto di Fisca dello Spazio Interplanetario, Spaz Interplnt/Area Ricerca CNR, Via Fosso del Cavaliere 100, Roma I-00133, Italy.

J. M. Bosqued, I. Dandouras, and H. Rème, Centre d'Etude Spatiale des Rayonnements, 9 avenue de Colonel Roche, Toulouse F-31028, France.

H. U. Frey, A. Keiling, G. K. Parks, and M. Wilber, Space Sciences Laboratory, 7 Gauss Way, University of California, Berkeley, CA 94720, USA. (keiling@ssl.berkeley.edu)

B. Klecker, Max-Planck-Institut für Extraterrestrische Physik, Giessenbachstrasse, Garching D-85741, Germany.

A. Korth, Max-Planck-Institut für Aeronomie, Sonnen System Forschung, Max-Planck-Str. 2, Katlenburg-Lindau D-37191, Germany.

R. Lundin, Swedish Institute of Space Physics, P. O. Box 812, Kiruna S-98128, Sweden.

M. McCarthy, School of Oceanography, University of Washington, Box 357940, Seattle, WA 98195-7940, USA.

C. Mouikis, Space Science Center, University of New Hampshire, Morse Hall, 39 College Road, Durham, NH 03824, USA.